Journal of Analytical and Applied Pyrolysis 164 (2022) 105526

Contents lists available at ScienceDirect

Journal of Analytical and Applied Pyrolysis

journal homepage: www.elsevier.com/locate/jaap

Pyrolysis characteristics of tea oil camellia (*Camellia oleifera* Abel.) shells and their chemically pre-treated residues: Kinetics, mechanisms, product evaluation and joint optimization

Peijun Chen [a], Chuanshuang Hu [a,*], Jin Gu [a], Xiuyi Lin [a], Chongling Yang [b], Shao-Yuan Leu [c], Litao Guan [a,*]

[a] College of Materials and Energy, South China Agricultural University, Guangzhou 510642, China
[b] Guangdong Industry Polytechnic, Guangzhou 510300, China
[c] Department of Civil & Environ. Engineering, the Hong Kong Polytechnic University, Hong Kong, China

ARTICLE INFO

Keywords:
Tea oil camellia
Pyrolysis
Kinetic analysis
TG-IR
Py-GC/MS

ABSTRACT

Tea oil camellia (*Camellia oleifera* Abel.) is a widely distributed oilseed plant in China that yielded around 3.14 million tons of camellia seeds in 2020. Consequently, millions of tons of tea oil camellia shells (TOCS) are produced as processing residues. They are mainly discarded or burned due to the lack of effective large-scale utilization strategies. In this study, the pyrolysis characteristics of raw/extracted/alkali-treated tea oil camellia shells (RTOCS/EXTOCS/ALTOCS) were elucidated via thermogravimetry-infrared spectroscopy, pyrolysis-gas chromatography/mass spectroscopy and artificial neural network (ANN) to demonstrate the application of TOCS in mass pyrolysis. The Coats–Redfern method was used for thermokinetic and thermodynamic analyses under different models. The 1.5-order reaction (F1.5) mechanism could best describe the main pyrolysis stages of RTOCS, EXTOCS and ALTOCS, with an activation energy of 40.14, 66.54 and 76.73 kJ/mol, respectively. Moreover, the pyrolysis gases were mainly released at 200–400 °C. EXTOCS pyrolysis produced more compounds containing C═O and C-O functional groups, while ALTOCS produced more CH_4. Nine types of organic compounds were identified. Multi-objective optimization based on ANN simulations indicated that ALTOCS pyrolysis at 800 °C was the optimal condition as it provided the highest pyrolysis efficiency. This study suggests that RTOCS, EXTOCS, and ALTOCS were suitable as biomass pyrolysis feedstocks. Therefore, this million-ton-level biomass is expected to serve full-component and high-value industrial utilization.

1. Introduction

Biomass is a renewable resource that can be converted into gaseous, liquid, and solid products. The exploitation of biomass resources can help reduce the use of non-renewable resources and the emission of greenhouse gases [1]. Lignocellulosic biomass represents the largest biomass feedstock on Earth, and it is mainly derived from agricultural and forestry waste. Generally, it is converted into industrial products such as chemicals or energy and materials [2].

Biomass pyrolysis is a thermochemical method that can be used to convert agricultural and forestry wastes into solid, gaseous, and liquid industrial products. Several factors can influence biomass pyrolysis characteristics of biomass pyrolysis, including biomass type, pyrolysis temperature, and the type of pyrolysis reactor. Therefore, the specific pyrolysis behavior and mechanisms should be analyzed to determine which characteristics should be applied for certain biomass [3].

Thermogravimetric analysis (TGA) combined with other techniques has been used to detect chemical changes in biomass during pyrolysis. Based on TGA, we can explore the relationship between biomass pyrolysis and temperature or time, and systematically investigate the pyrolysis kinetics, while providing a theoretical basis of thermochemical conversion system design [4]. The thermogravimetry-infrared spectroscopy (TG-IR) system integrates TG and FTIR to simultaneously detect the composition of pyrolysis gases, such as H_2O, CH_4, H_2, CO_2, and other cracking gases, as the temperature increases. Pyrolysis-gas chromatography/mass spectrometry (Py-GC/MS) can also be used for biomass characterization. It can effectively identify volatile products generated during pyrolysis based on the analysis of peak areas [5].

* Corresponding authors.
E-mail addresses: cshu@scau.edu.cn (C. Hu), ltguan@scau.edu.cn (L. Guan).

https://doi.org/10.1016/j.jaap.2022.105526
Received 22 December 2021; Received in revised form 7 April 2022; Accepted 13 April 2022
Available online 16 April 2022

Because pyrolysis includes complex reactions, TG-IR and Py-GC/MS are often combined to assess the pyrolysis behavior and products of biomass residues [6].

Tea oil camellia (*Camellia oleifera* Abel.) is an oil plant of the genus *Camellia* of the family Theaceae, with a long history as a crop, high economic value, and wide plantation area. Notably, it is considered one of the world's four major woody oilseed species [7]. Tea oil camellia is widely distributed in China, Japan, Southeast Asia, as well as other countries and regions. The annual production of tea oil camellia seeds in China reached 3.14 million tons [8]. During the shell-seed separation of tea oil, 0.54 tons of waste shells are produced for every ton of tea oil camellia fruit [9]. In 2020, China produced approximately 3.68 million tons of tea oil camellia shells (TOCS). These TOCS are usually burned as biomass waste, thereby causing air and water pollution [10,11].

The chemical composition of TOCS is complex, and it includes a variety of active organic compounds that can be extracted by different solvents. Water, alcohols, and acetone can be used as solvents to extract oligosaccharide [12], tea polyphenols [13], and flavonoids [14], whereas hemicellulose [15], insoluble dietary fiber [16], xylose and vanillin [17] can be extracted by NaOH treatments. TOCS extracts can be used as a natural skin-whitening agent in cosmetic products [18]. Current research on TOCS utilization focuses mostly on the extraction and chemical transformation of active ingredients based on the extraction and preparation of single chemicals from certain TOCS components. However, these methods are not practically associated with a resourceful utilization of large amounts of this chemically pre-treated residue. They also become a new kind of intractable waste [12,14]. Currently, applications of pyrolysis technology using chemically pre-treated residues of TOCS are still at the research and development stage, and the theoretical background thereof is being established.

Thermal treatment methods such as pyrolysis and gasification are promising as they enable rapid waste reduction while generating energy or valuable by-products [19]. Deng et al. [20] mixed TOCS and solid waste with a mass ratio of 3:7 and found that the apparent activation energy was the lowest when HZSM-5 and CaO were used as catalysts for pyrolysis at 700 °C. Zhang et al. [21] investigated the pyrolysis properties of TOCS, coal and their mixtures using a thermogravimetric analyzer and a fixed bed reactor. The decomposition reactions and kinetic analysis of TOCS, coal and their mixtures were compared. Fan et al. [22] investigated the characteristics of the three different types of biochar obtained via the hydrothermal carbonization, torrefaction, and pyrolysis of TOCS. The biochar produced by pyrolysis had superior physicochemical properties, which could substitute lignite or semi-anthracite coal. Zhang et al. [23] performed a combination of foam drying and pyrolysis of sewage sludge with the addition of TOCS biochar to investigate the effect of process parameters on foam drying and the characteristics of the biochar produced. However, there are still gaps in the knowledge of how the pyrolytic properties, kinetics and performance of TOCS changes in terms of chemical pretreatment. The changes in their gaseous products with temperature remain poorly elucidated and joint optimization of pyrolysis process has not been addressed.

In this study, the kinetic and thermodynamic parameters of TOCS and their chemically pre-treated residues were comprehensively analyzed using TGA. The pyrolysis gases were analyzed using TG-IR and Py-GC/MS systems. To the best of our knowledge, this is the first study to employ an ANN model to optimize the thermal decomposition conditions of TOCS. Analytical results revealed the pyrolysis behaviors of RTOCS, their extracted and alkali-treated residues to provide theoretical guidance for the design and manufacture of pyrolysis systems applicable to this million-ton-level biomass waste.

2. Materials and methods

2.1. Experimental materials

TOCS were harvested from a tea oil camellia plantation of Guangdong Shanma Agricultural and Forestry Development Co., Ltd., in Lianzhou City, Guangdong Province, China. They were naturally dried, bagged and stored in a sealed container protected from light. TOCS were powdered using a cutting crusher, and the obtained shell powder was screened to a particle size below 450 μm.

TOCS extracted with benzene/ethanol and hot water were defined as extracted TOCS (EXTOCS), while TOCS extracted with benzene/ethanol, hot water, and alkali treatment were defined as alkali-treated TOCS (ALTOCS). The raw TOCS samples were defined as RTOCS.

The organic extracts of TOCS were removed by performing Soxhlet extraction for 6 h according to the Chinese standard GB/T 2677.6–94, with 150 mL of a benzene: ethanol solution exhibiting a volume ratio of 2:1. To remove the hot water-soluble extracts, 2 g of TOCS were soaked in 200 mL of hot boiling ultrapure water (HW) for 3 h according to GB/T 2677.4–93. For the alkali treatment, 2 g of EXTOCS were soaked in 100 mL of a boiling 1% sodium hydroxide solution for 1 h and washed with an acetic acid solution according to GB/T 2677.5–93.

2.2. Determination of components

Proximate analysis was performed using an elemental analyzer. The volatile and ash contents were determined according to the standard test methods ASTM D3175–11 and ASTM D3174–12, respectively. The calculation method used for fixed carbon was to subtract the volatile and ash contents from the initial value. An ultimate analysis was conducted using an element analyzer (vario EL cube, Elementar, Germany). The higher heating value (HHV) of the feedstock was calculated according to Dulong's formula [24]: HHV (MJ/kg) = 0.338 C + 1.428(H-O/8) + 0.095 S, where C, H, O, and S are the weight percentages of the respective elemental components.

2.3. Determination of thermogravimetric characteristics

For the thermogravimetric analysis, the TG209F1 Libra thermogravimetric analyzer (NETZSCH, Germany) was used. A sample of approximately 5 mg was loaded into an alumina crucible and heated from 100° to 800°C at a heating rate of 10 °C/min under nitrogen protection at a 20 mL/min flow rate.

2.4. Kinetic study

The kinetics of most reactions can be summarized as follows:

$$\frac{d\alpha}{dt} = Kf(\alpha) \tag{1}$$

where $\alpha = (M_0 - M_t)/(M_0 - M_\infty)$; M_0 is the initial sample mass; M_t is the sample mass at time t; M_∞ is the final sample mass; f(α) is a function of α and K is the Arrhenius rate constant.

The Arrhenius equation is given by:

$$K = Ae^{\frac{-E}{RT}} \tag{2}$$

where T is the absolute temperature, (in Kelvin); A is the pre-exponential factor, s^{-1}; E is the activation energy, kJ·mol^{-1}; and R is the universal gas constant (R=0.0083145 kJ·mol^{-1}·K^{-1}).

Moreover, $f(\alpha) = (1-\alpha)^n$ and n is the reaction order. For the heating rate $\beta = \frac{dT}{dt}$, Combining Eqs. (1) and (2), we obtained the basic equation of the TG curve:

$$\frac{d\alpha}{dT} = \frac{A}{\beta}e^{(-E/RT)}(1-\alpha)^n \tag{3}$$

Finally, g(α) is an integral form of the reaction model [25] and is defined as:

$$g(\alpha) = \int_0^\alpha \frac{d(\alpha)}{f(\alpha)} = \frac{A}{\beta}\int_{T_0}^{T} e^{(\frac{-E}{RT})}dT \tag{4}$$

Table 1
Common reaction models of g(α) and f(α) functions [15,25].

Reaction model	Reaction mechanism		g (α)	f (α)
Chemical reaction	First-order reaction	F1	-ln(1-α)	1-α
	1.5-order reaction	F1.5	$2[(1-\alpha)^{-1/2}-1]$	$(1-\alpha)^{3/2}$
	Second-order reaction	F2	$(1-\alpha)^{-1}$	$(1-\alpha)^{2}$
Diffusion-controlled reaction	One-dimensional diffusion	D1	α^2	1/2α
	Two-dimensional diffusion	D2	(1-α)ln(1-α)+α	$-\ln(1-\alpha)^{-1}$
	Three-dimensional diffusion	D3	$[1-(1-\alpha)^{1/3}]^2$	$3(1-\alpha)^{2/3}[1-(1-\alpha)^{1/3}]^{-1/2}$
Phase boundary reaction	One-dimensional	R1	α	1
	Two-dimensional	R2	$1-(1-\alpha)^{1/2}$	$2(1-\alpha)^{1/2}$
	Three-dimensional	R3	$1-(1-\alpha)^{1/3}$	$3(1-\alpha)^{2/3}$

where T_0 is the initial temperature.

2.4.1. Kinetic equation

The Coats–Redfern method is widely used to investigate the kinetics of pyrolysis and analyze the corresponding kinetic parameters, such as activation energy and pre-exponential factors [26]. This integral method was obtained by approximating the temperature integral.

The approximate inductive integration of temperature by Eq. (4) yielded the Coats–Redfern equation:

$$\ln[\frac{g(\alpha)}{T^2}] = \ln[\frac{AR}{\beta E}(1-\frac{2RT}{E})] - \frac{E}{RT} \quad (5)$$

Moreover, because $2RT/E \ll 1$, there was a linear relationship between $\ln[g(\alpha)/T^2]$ and $(1/T)$ in Eq. (5). It is noteworthy that reaction models present different definitions of $g(\alpha)$ (Table 1). When those definitions of g(α) fit to Eq. (5), different values of activation energy (E) and frequency factor (A) will be given using the Origin software.

2.4.2. Determination of thermodynamic parameters

Isotransformation kinetic models were used to determine thermodynamic parameters, including the pre-exponential factor (A) in the Arrhenius equation, enthalpy (ΔH), Gibbs free energy (ΔG), and entropy changes (ΔS) [27]:

$$A = \frac{\beta E e^{\frac{E}{RT_m}}}{RT_m^{\ 2}} \quad (6)$$

$$\Delta H = E - RT, \quad (7)$$

$$\Delta G = E + RT_m \ln(\frac{kT_m}{hA}), \quad (8)$$

$$\Delta S = \frac{\Delta H - \Delta G}{T_m}, \quad (9)$$

where k is the Boltzmann constant (1.381×10^{-23} J/K), h is the Planck constant (6.626×10^{-34} J•s) and T_m is the DTG peak temperature.

2.5. Thermogravimetry-infrared spectroscopy experiments

The gas products released during pyrolysis were analyzed using the thermogravimetric analyzer (TG 209 F1, NETZSCH, Germany) combined with an FTIR spectrometer (Nicolette IS 50, Thermo Fisher Scientific, USA). TOCS were heated from 35° to 800°C at a heating rate of 10 °C/min under an inert nitrogen atmosphere flowing at 50 mL/min. The gas escaping the TGA pyrolyzer was transferred to the gas chamber of the FTIR spectrometer through a heated transmission line and recorded with a 4 cm^{-1} resolution over a spectral range of 4000–400 cm^{-1}. To prevent condensation of the escaping gas, the temperature in the conveying line and gas chamber was maintained at 280 °C.

2.6. Pyrolysis-gas chromatography/mass spectrometry experiments

The Py-GC/MS system was composed of a multi-pyrolysis device (EGA/PY-30D, Frontier Laboratories, Japan) and a gas chromatograph-mass spectrometer (GCMS-QP-2010, Shimadzu, Japan). TOCS were rapidly pyrolyzed at 500 °C using high-purity helium as the protective gas. The resulting gaseous products were introduced into the injection port of the gas chromatograph (separation ratio 1:80), and then entered the capillary column (Agilent J&W DB-5, 30 m × 0.25 mm × 0.25 μm) for chromatographic separation. The interface temperature was maintained at 300 °C, whereas the injector was maintained at 275 °C. The mass spectrometer was operated in the electron ionization (EI) mode at 70 eV. Finally, the chromatographic peaks were identified based on the NIST database.

2.7. Multi-objective optimization of thermal decomposition using an artificial neural network

Artificial neural networks are a mathematical technique used to model complex nonlinear problems and can accurately evaluate the nonlinear relationships between multiple input and output data, and have been successfully applied to TG data [28]. In this study, ANN was used to fit a multiple regression model of mass retention (%) and DTG (%/min) as a function of sample type (RTOCS/EXTOCS/ALTOCS), temperature (°C), and heating rate (°C/min). The optimization objective is to minimize the mass retention and maximize the DTG to increase the pyrolysis efficiency based on the multiple regression model. The ANN hyperparameters were chosen based on the root mean square error (RMSE), and correlation coefficient (R^2) derived from random 5-fold cross-validation (n = 12585). Ultimately, the composite desirability (D) was maximized to obtain the joint optimization of the responses [19,29]. The ANN analysis was performed using the software JMP Pro 16.1.

3. Results and discussion

3.1. Characterization of tea oil camellia shells

The ultimate and proximate analyses and the HHV values of TOCS are shown in Table 2. The ultimate analysis showed that N and S contents in TOCS were 0.13–0.24 wt% and 0.11–0.36 wt%, respectively. They indicate low NO_x and SO_2 emissions during pyrolysis. In addition, the RTOCS, EXTOCS, and ALTOCS exhibited HHV values of 17.73,

Table 2
Proximate and Ultimate analysis of TOCS.

	RTOCS[a]	EXTOCS[a]	ALTOCS[a]	RTOCS[b] from Jiangxi
Proximate analysis (wt%)				
Volatile matter	71.74	83.95	84.49	68.42
Fixed carbon	26.32	14.62	15.00	24.12
Ash	1.94	1.43	0.51	2.64
Ultimate analysis(wt %)				
Carbon	48.08	48.78	48.07	47.66
Hydrogen	6.65	6.77	6.77	5.95
Nitrogen	0.21	0.24	0.13	0.46
Sulphur	0.11	0.20	0.36	0.39
Oxygen[c]	44.95	44.02	44.67	44.06
HHV(MJ/kg)	17.73	18.31	17.98	17.00
Reference	This study	This study	This study	[21]

[a] oven-dried basis;
[b] air-dried basis;
[c] by-difference

18.31, and 17.98 MJ/kg, respectively. The volatile matter content of TOCS was determined as 71.74 wt%. This high volatile matter content was advantageous for the formation of liquid and gaseous products by pyrolysis. During the pyrolysis process, biomasses with high ash content can lead to several issues, including agglomeration, fouling, and slagging in the presence of inorganic minerals (alkaline and alkaline soils), affecting the pyrolysis efficiency [3]. Therefore, their fairly low ash content (0.51–1.94 wt%) can effectively avoid this problem. The results of the proximate and ultimate analyses in this study were similar to the results of analyses conducted on RTOCS of different origins, as reported in the literature [21]. They all have low ash, N and S contents, suggesting that both RTOCS and their pretreatment residues can be considered suitable pyrolysis feedstock.

3.2. Thermogravimetric analysis

The thermogravimetric and differential thermogravimetric curves of the pyrolysis of the three TOCS at a heating rate of 10 °C/min are shown in Fig. 1. This pyrolysis process can be divided into three stages: volatilization, main components decomposition and residual decomposition stage. In the first stage (100–220 °C), the mass loss was primarily attributed to the volatilization of moisture and low boiling point components. EXTOCS and ALTOCS presented mass losses of only 0.76% and 1.25%, respectively, showing their good thermal stability at this stage. In the second stage (220–400 °C), the mass losses of RTOCS, EXTOCS, and ALTOCS were 48.64%, 60.48%, and 65.4%, respectively. The temperature ranges for the decomposition of hemicellulose, cellulose, and lignin have been reported as 225–350 °C, 325–375 °C, and 250–500 °C, respectively [5]. All three samples showed a sharp weight loss starting at 220 °C, likely attributable to the onset of hemicellulose decomposition. They also showed two DTG peaks at this stage. The maximum weight loss peaks of RTOCS, EXTOCS, and ALTOCS were observed at 273, 293, and 300 °C, whereas the second weight loss peaks were observed at 327, 344, and 336 °C, respectively. The left and right DTG peaks marked rapid hemicellulose and cellulose degradation, respectively. In the third stage (400–800 °C), it seemed to be slow thermal degradation of residues such as char, minerals and ash that are part of the final solid residue. The residual rate of RTOCS at 800 °C was 33.51%, which was higher than the 27.60% of EXTOCS and 23.16% of ALTOCS indicating that both ALTOCS and EXTOCS could be degraded more fully than the RTOCS.

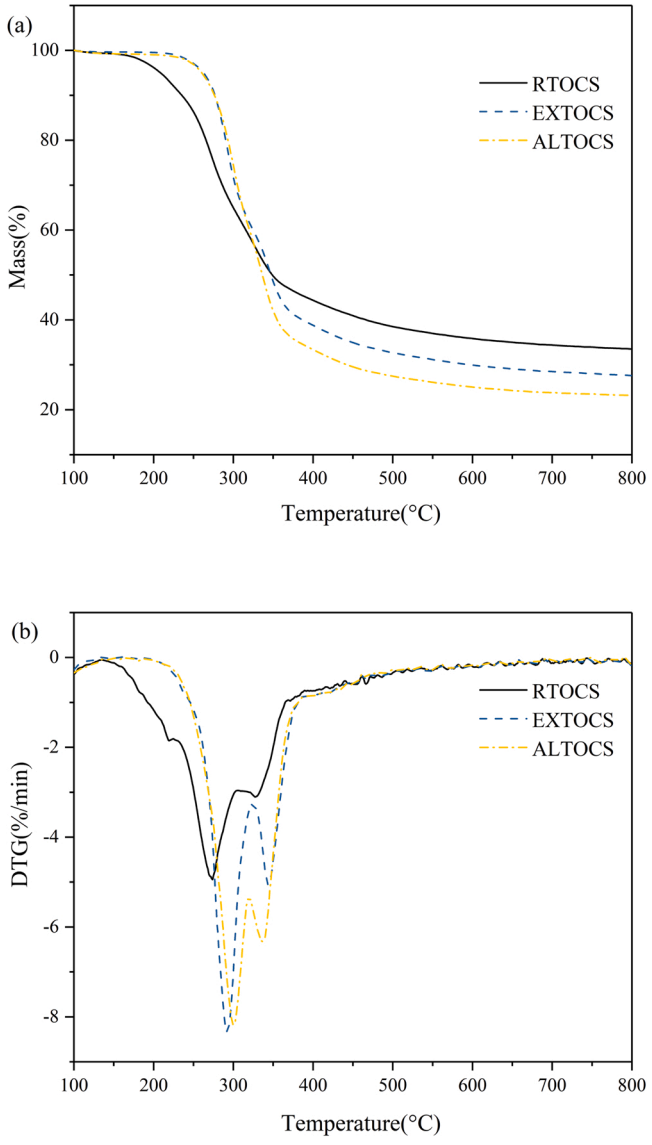

Fig. 1. Pyrolysis of RTOCS, EXTOCS, and ALTOCS at 10 °C/min: (a) TG curve, and (b) DTG curve.

3.3. Kinetic and thermodynamic characteristics

The Coats–Redfern model was applied to describe the main thermal decomposition stages (250–350 °C) of TOCS (Table 3). Various types of kinetic models corresponding to the observed kinetic mechanisms, activation energy, and correlation coefficients (R) were identified. For RTOCS, EXTOCS, and ALTOCS samples, the 1.5-order reaction (F1.5) presented the highest correlation coefficients (R) and the best linearity. Therefore, F1.5 was considered the mechanism model with the best fit. In addition, F1, D2, D3, and R3 also presented high correlation coefficients with the three TOCS samples, which suggests that these reaction models might also describe the pyrolysis reaction to a certain extent.

The activation energy is the minimum energy required to initiate a reaction. Therefore, reactions with high activation energies require high temperatures or long reaction times [30]. Based on the F1.5 model, the activation energies of RTOCS, EXTOCS, and ALTOCS were 40.14, 66.54, and 76.73 kJ/mol, respectively. Therefore, EXTOCS and ALTOCS were more thermally stable than RTOCS.

The activation energies of the three TOCS samples were compared with those of different types of agroforestry wastes at similar pyrolysis temperatures under the F1 model (Table 4). RTOCS presented the lowest activation energy (31.55 kJ/mol). The activation energy of EXTOCS and ALTOCS was similar to that of sugar cane residue (60.53 kJ/mol). Because of its low cellulose content [31], the activation energy of TOCS was substantially lower than that of walnut, almond, and pistachio shells (109.83–147 kJ/mol). This difference occurred because biomass with high cellulose contents often requires higher activation energy to decompose [32].

The thermodynamic parameters (ΔH, ΔS, ΔG) of the three TOCS under different reaction mechanism models are shown in Table 3. Enthalpy (ΔH) is a state function reflecting the amount of heat absorbed or released in a chemical reaction, and it also shows the chemical bond dissociations at a constant pressure [33]. For the three TOCS, the difference between the activation energy and ΔH was only 4–5 kJ/mol. These results indicate that the potential energy barriers required for the reaction were low, which was favorable for forming the activated complex [34]. Entropy (ΔS) is a state function that represents the disorder of a system. The negative values of ΔS for different reaction models (−0.28 to −0.07 kJ/mol) confirmed that the pyrolysis products presented a more organized structure, less disorder, and higher energy than the initial materials [35]. The change in Gibbs free energy (ΔG) reflects the increase in the total energy of a system as the reagent reacts and the activated complex is formed [36]. The ΔG value of ALTOCS (169.13 kJ/mol) was similar to that of EXTOCS (167.27 kJ/mol), which

Table 3
Thermokinetic and thermodynamic analysis based on the Coats–Redfern model.

Samples	Reaction model	Fitted equation	R^2	E (kJ/mol)	ΔH (kJ/mol)	ΔG (kJ/mol)	ΔS (kJ/mol•K)
	F1	y = −3794.23x-6.31	0.9801	31.55	27.00	164.67	-0.25
	F1.5	y = −4828.40x-4.28	0.9915	40.14	35.60	163.58	-0.23
	F2	y = −2715.27x-7.09	0.9790	22.57	18.03	166.19	-0.27
	D1	y = −5424.92x-4.49	0.9485	45.10	40.56	163.05	-0.22
RTOCS	D2	y = −6356.53x-3.31	0.9637	52.85	48.30	162.33	-0.21
	D3	y = −7507.04x-2.53	0.9770	62.41	57.87	161.57	-0.19
	R1	y = −2141.34x-9.59	0.9169	17.80	13.26	167.27	-0.28
	R2	y = −2899.65x-8.77	0.9579	24.11	19.56	165.90	-0.27
	R3	y = −3182.40x-8.62	0.9669	26.46	21.91	165.47	-0.26
EXTOCS	F1	y = −6937.14x-1.30	0.9701	57.68	52.97	167.94	-0.20
	F1.5	y = −8003.61x+0.72	0.9786	66.54	61.84	167.27	-0.19
	F2	y = −2909.37x-7.01	0.9387	24.19	19.49	172.03	-0.27
	D1	y = −11390.30x+5.19	0.9522	94.70	90.00	165.61	-0.13
	D2	y = −12465.32x+6.55	0.9605	103.64	98.94	165.19	-0.12
	D3	y = −13713.63x+7.43	0.9685	114.02	109.31	164.74	-0.10
	R1	y = −5124.08x-4.75	0.9407	42.60	37.90	169.37	-0.23
	R2	y = −5977.86x-3.82	0.9576	49.70	45.00	168.64	-0.22
	R3	y = −6285.75x-3.64	0.9622	52.26	47.56	168.41	-0.21
ALTOCS	F1	y = −8061.25x+0.54	0.9930	67.02	62.25	169.77	-0.19
	F1.5	y = −9229.44x+2.74	0.9948	76.73	71.97	169.13	-0.17
	F2	y = −3289.14x-6.37	0.8699	27.35	22.58	174.04	-0.26
	D1	y = −13311.76x+8.34	0.9811	110.67	105.91	167.38	-0.11
	D2	y = −14479.81x+9.85	0.9867	120.39	115.62	166.98	-0.09
	D3	y = −15841.35x+10.91	0.9913	131.70	126.94	166.55	-0.07
	R1	y = −6084.76x-3.18	0.9770	50.59	45.82	171.11	-0.22
	R2	y = −7013.76x-2.12	0.9873	58.31	53.55	170.43	-0.20
	R3	y = −7349.55x-1.89	0.9897	61.10	56.34	170.21	-0.20

Table 4
Activation energy of different biomass feedstock at 10 °C/min according to the F1 model.

Samples	Temperature	E (kJ/mol)	Reference
Sewage sludge	240–330	29.34	[44]
sugar cane residue	250–360	60.53	[45]
walnut shell	215–370	109.83	[46]
almond shell	197–330	130.69	[47]
pistachio shell	239–337	147	[48]
Raw tea oil camellia shell	250–350	31.55	This study
Extracted tea oil camellia shell	250–350	57.68	This study
Alkali-treated camellia shell	250–350	67.02	This study

was slightly higher than that of TOCS (163.58 kJ/mol), as calculated by the F1.5 model. This finding reflects the bioenergy potential of TOCS.

3.4. Thermogravimetric-infrared spectrometry results

The gas yield from evaporation during the pyrolysis can be predicted based on FTIR absorbance height or area. To identify the emission profiles of specific volatiles, their characteristic absorption peaks were extracted from the 3D FTIR spectra, as shown in Fig. 2. These peaks occurred at 3579, 2953, 2358, 2185, 1795, and 1182 cm^{-1} (Table 5), which corresponded mainly to H_2O, CH_4, CO_2, CO, compounds containing C═O bonds (acids, aldehydes, ketones, ethers), and compounds containing C-O bonds (alcohols, phenols, ethers), respectively.

The peak in the 4000–3500 cm^{-1} band indicated the release of H_2O [37]·H_2O mainly originated from the precipitation of free, bound, and crystalline water in the sample minerals and the cleavage or reaction of oxygen-containing functional groups with increasing temperature during pyrolysis [38]. The absorption peak at 3000 − 2850 cm^{-1} was associated with the CH_4 release, whereas at 2400–2240 cm^{-1} was associated with CO_2 release. The CH_4 release was mainly due to the cleavage of methoxy group. The CO_2 release was due to the cleavage and reorganization of carboxyl and -COOH functional groups, which cleaved and shed the C-C and C-O bonds attached to the main hemicellulose branched chains, thereby cleaving the C═O group from the cellulose [39]. Absorption peaks at 1850 − 1600 cm^{-1} of C═O corresponded to aldehydes, acids, and ketones produced by the cleavage of epoxy groups. The absorption peaks at 1300 − 900 cm^{-1} were attributed to hydroxyl compounds [40]. EXTOCS presented the strongest intensity of C═O compounds, C-O compounds, and H_2O release, whereas ALTOCS presented the most intense CH_4 release. The peak intensity of a specific wavenumber represents the concentration of released pyrolysis products [41]. For these particular volatile emission profiles, most emissions occurred at 200 − 400 °C, with two main absorption peaks near 306 and 360 °C for EXTOCS and near 313 °C and 357 °C for ALTOCS. The temperatures of these two major absorption peaks were similar to the peaks in the DTG profile.

3.5. Pyrolysis-gas chromatography/mass spectrometry analysis

The ionic intensities of gases produced by the pyrolysis were analyzed using Py-GC/MS, as shown in Table 6. Following the NIST library, 30 organic compounds were identified in the pyrolysis gases. They were classified into nine categories based on functional groups: acids, alcohols, aldehydes, aromatics, esters, furans, ketones, nitrogenous compounds, and phenols. Among them, acids and ketones are known to be mainly produced by hemicellulose degradation, whereas phenols are primarily produced by lignin degradation [42]. The chromatographic peak areas of the compounds showed a linear relationship with the compound content [43]. The thermal cleavage of RTOCS and EXTOCS produced mainly acids and phenols, whereas the thermal cleavage of ALTOCS did not produce acids and yielded more ketones (27.66%). The pyrolysis products of RTOCS, EXTOCS, and ALTOCS all showed a phenol content exceeding 25%. Both extraction and alkali treatments significantly affected the phenolic species and content distribution. The extraction negatively affected the phenolic production of 2-methoxy-phenol, 2,6-dimethoxy-phenol, and 4-ethenyl-2-methoxy--phenol and produced 7.63% of 4-methoxy-3-(methoxymethyl)-phenol. Moreover, the alkali treatment led to the formation of 4-methoxy-phenol, 3,4-dimethoxy-phenol, and trans-isoeugenol cleavage products.

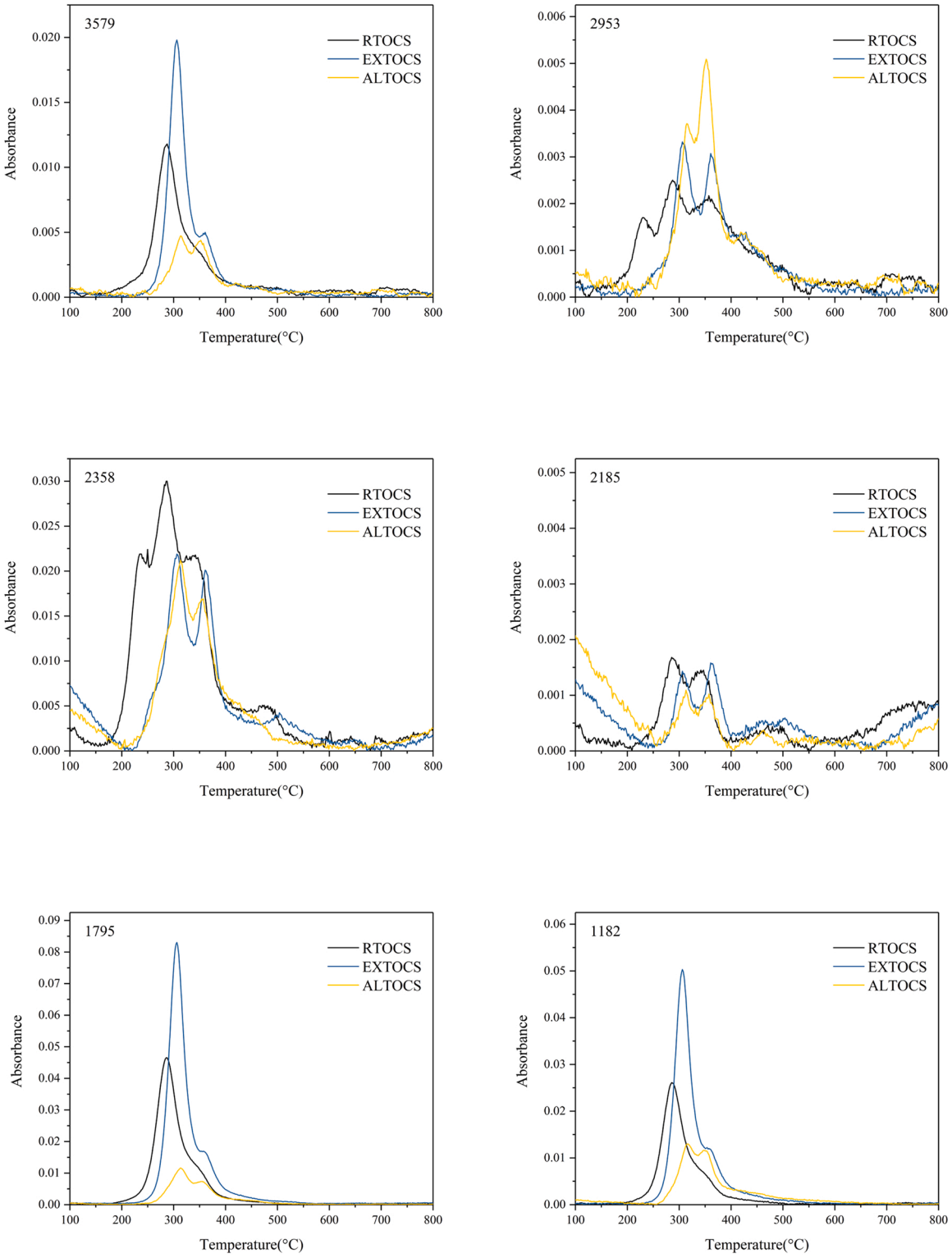

Fig. 2. Infrared absorption spectra of the main pyrolysis products of the samples at different temperatures.

Table 5
Summary of selected functional groups for analysis of gaseous products using TG-IR [39,40].

Wavenumber (cm^{-1})	Functional group	Possible compounds
4000–3500	O-H	H_2O, alcohol, phenols
3000–2850	C-H	CH_4
2400–2240;780–560	O═C═O	CO_2
2240–2060	C-O	CO
1850–1600	C═O	Acids, aldehydes, ketones, ethers
1300–900	C-O	Alcohols, phenols, ethers

3.6. Optimization of pyrolysis conditions using an artificial neural network

By using the trial-and-error method, the ANN hyperparameters are determined with two hidden layers, each with eight neurons and the hyperbolic tangent (TanH) was chosen as activation function. The architecture of ANN (3 × 8 × 8 × 2) is shown in Fig. 3 and the performance metrics are given in Table 7. According to the ANN-based joint optimization (Fig. 4), the optimum operating conditions were obtained using an ALTOCS sample at a temperature of 800 °C and a heating rate of 20 °C/min, which resulted in a maximum composite agreement (D) of

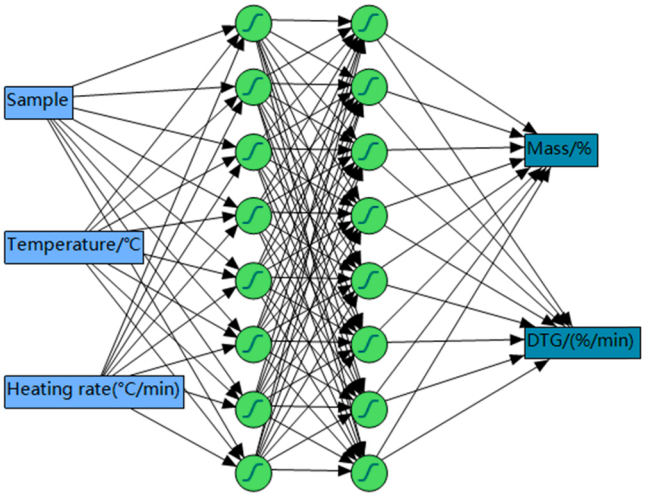

Fig. 3. Structure of artificial neural network in this study.

Table 6
Classification and peak area percentage of TOCS pyrolysis products based on Py-GC/MS.

Compounds	Formula	peak area (%)		
		RTOCS	EXTOCS	ALTOCS
Acids				
Acetic acid	$C_2H_4O_2$	**37.81 ± 4.37%**	**34.23 ± 5.77%**	
Alcohols				
Cyclobutanol	C_4H_8O		**1.19 ± 0.16%**	
Aldehydes				
4-Methyl-2,5-dimethoxybenzaldehyde	$C_{10}H_{12}O_3$	**2.68 ± 0.71%**	**1.89 ± 0.16%**	
Aromatics				
Benzene, 1,2,3-trimethoxy-5-methyl-	$C_{10}H_{14}O_3$	**1.58 ± 0.19%**		**1.24 ± 0.45%**
Esters				
Acetic acid, methyl ester	$C_3H_6O_2$		0.32 ± 0.01%	
Acetic acid, ethenyl ester	$C_4H_6O_2$	1.66 ± 0.03%		
Total		**1.66%**	**0.32%**	
Furans				
Furfural	$C_5H_4O_2$		4.87 ± 0.04%	10.34 ± 4.37%
Furan, 2-methyl-	C_5H_6O	1.19 ± 0.07%		
5-Isopropyl-3,3-dimethyl-2-methylene-2,3-dihydrofuran	$C_{10}H_{16}O$		6.14 ± 0.06%	
Total		**1.19%**	**11.01%**	**10.34%**
Ketones				
2-Propanone, 1-hydroxy-	$C_3H_6O_2$	0.60 ± 0.13%		
2,3-Butanedione	$C_4H_6O_2$			7.53 ± 2.98%
2-Cyclopenten-1-one	C_5H_6O	4.37 ± 2.59%		
1,2-Cyclopentanedione	$C_5H_6O_2$			9.53 ± 4.86%
2-Propanone, 1-(acetyloxy)-	$C_5H_8O_3$	1.05 ± 0.03%	0.79 ± 0.48%	1.23 ± 0.45%
1,2-Cyclopentanedione, 3-methyl-	$C_6H_8O_2$		2.29 ± 0.55%	
2-Cyclopenten-1-one, 2-hydroxy-3-methyl-	$C_6H_8O_2$			2.22 ± 0.52%
4-Hydroxy-3-methylacetophenone	$C_9H_{10}O_2$			7.15 ± 2.32%
Total		**6.02%**	**3.08%**	**27.66%**
Nitrogenous compounds				
Oxazolidine, 2,2-diethyl-3-methyl-	$C_8H_{17}NO$		1.77 ± 0.34%	3.16 ± 0.73%
Benzeneethanamine, 3,4,5-trimethoxy-	$C_{11}H_{17}NO_3$		1.21 ± 0.01%	
Total			**2.98%**	**3.16%**
Phenols				
Phenol, 2-methoxy-	$C_7H_8O_2$	6.46 ± 0.74%	3.82 ± 0.39%	
Phenol, 4-methoxy-	$C_7H_8O_2$			3.07 ± 0.37%
Phenol, 2-methoxy-4-methyl-	$C_8H_{10}O_2$	3.84 ± 0.59%	4.59 ± 0.31%	3.45 ± 0.59%
Phenol, 2,6-dimethoxy-	$C_8H_{10}O_3$	7.76 ± 0.56%	5.09 ± 0.82%	8.21 ± 2.38%
Phenol, 3,4-dimethoxy-	$C_8H_{10}O_3$			3.25 ± 1.27%
Phenol, 4-ethenyl-2-methoxy-	$C_9H_{10}O_2$	8.47 ± 0.54%	5.87 ± 2.34%	
Phenol, 4-ethyl-2-methoxy-	$C_9H_{12}O_2$	2.29 ± 0.45%		2.33 ± 0.64%
Phenol, 4-methoxy-3-(methoxymethyl)-	$C_9H_{12}O_3$		7.63 ± 0.60%	
Phenol, 2-methoxy-4-propenyl-, (*Z*)-	$C_{10}H_{12}O_2$	0.52 ± 0.07%		
trans-Isoeugenol	$C_{10}H_{12}O_2$			4.76 ± 1.17%
Phenol, 2,6-dimethoxy-4-(2-propenyl)-	$C_{11}H_{14}O_3$	4.26 ± 0.88%	4.25 ± 0.40%	
Total		**33.6%**	**31.25%**	**25.07%**

Table 7
The ANN model performance used in this study.

Response	Training		Validation	
	Measures	Value	Measures	Value
Mass(%)	n	10068	n	2517
	R^2	0.9999	R^2	0.9999
	RMSE	0.0980	RMSE	0.0977
DTG(%/min)	n	10068	n	2517
	R^2	0.9861	R^2	0.9869
	RMSE	0.2688	RMSE	0.247

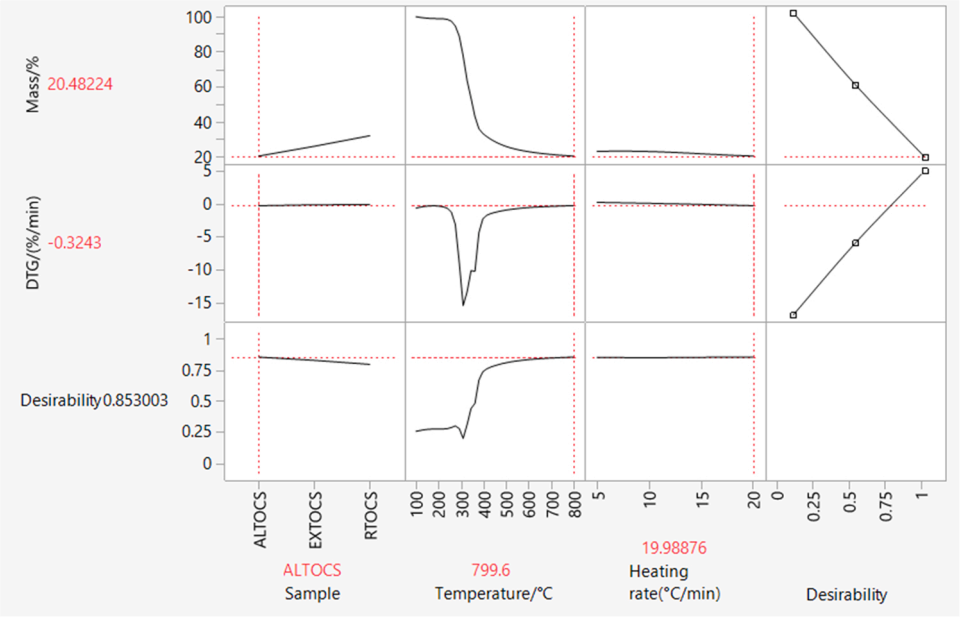

Fig. 4. Multi-objective optimization of pyrolysis efficiency, where the red numbers and dashed lines indicate the values taken for this optimization condition.

0.853. Above 700 °C, the increase in temperature had a minor effect on composite agreement. Finally, Monte Carlo resampling simulations were used to determine the contribution of each factor to the variability of composite agreement. Temperature was found to be the primary driver for all reactions, and sample type affected the mass curve almost exclusively.

4. Conclusions

The thermal analysis revealed the pyrolysis potential of RTOCS, EXTOCS and ALTOCS to be comparable to conventional biomass raw materials, with the advantages of low activation energy, low nitrogen and sulfur contents. The pyrolysis gas products included nine types of organic compounds, and the main gaseous products were obtained at low temperatures (200–400 °C). Multi-objective optimization based on an ANN indicated that ALTOCS pyrolysis at 800 °C was the optimal condition. RTOCS, their extracted and alkali-treated residues that are currently burned or landfilled are expected to be resourcefully utilized as a raw material for producing bioenergy and green chemicals, thus offering a high-value utilization opportunity for all components of this million-ton-level biomass.

CRediT authorship contribution statement

Peijun Chen: Conceptualization, Methodology, Software, Writing – original draft. **Chuanshuang Hu:** Investigation, Project administration, Resources. **Jin Gu:** Formal analysis, Supervision. **Xiuyi Lin:**Investigation, Data curation. **Chongling Yang:** Resources, Funding acquisition. **Shao-Yuan Leu:** Validation, Formal analysis. **Litao Guan:** Investigation, Conceptualization, Funding acquisition, Writing – review & editing.

Declaration of Competing Interest

The authors declare that they have no known competing financial interests or personal relationships that could have appeared to influence the work reported in this paper.

Acknowledgments

This project was financially supported by the Guangdong Provincial Department of Science and Technology, China (Project No. 2019A0 50503009, No. 2022A1515010502 and No. 2020A1515111106), the Bureau of Guangdong Forestry, China (Project No. 2020KJCX008) and the Science and Technology Program of Guangzhou, China (Project No. 202002030362).

Appendix A. Supporting information

Supplementary data associated with this article can be found in the online version at doi:10.1016/j.jaap.2022.105526.

References

[1] S. Mekhilef, R. Saidur, A. Safari, W.E.S.B. Mustaffa, Biomass energy in Malaysia: current state and prospects, Renew. Sust. Energy Rev. 15 (2011) 3360–3370, https://doi.org/10.1016/j.rser.2011.04.016.

[2] L. Zhang, Y. He, Y. Zhu, Y. Liu, X. Wang, Camellia oleifera shell as an alternative feedstock for furfural production using a high surface acidity solid acid catalyst, Bioresour. Technol. 249 (2018) 536–541, https://doi.org/10.1016/j.biortech.2017.10.061.

[3] M.H. Tahir, M.A. Mahmood, G. Çakman, S. Ceylan, Pyrolysis of oil extracted safflower seeds: Product evaluation, kinetic and thermodynamic studies, Bioresour. Technol. 314 (2020), 123699, https://doi.org/10.1016/j.biortech.2020.123699.

[4] F. Sher, S.Z. Iqbal, H. Liu, M. Imran, C.E. Snape, Thermal and kinetic analysis of diverse biomass fuels under different reaction environment: a way forward to renewable energy sources, Energy Convers. Manag. 203 (2020), 112266, https://doi.org/10.1016/j.enconman.2019.112266.

[5] N. Gao, A. Li, C. Quan, L. Du, Y. Duan, TG–FTIR and Py–GC/MS analysis on pyrolysis and combustion of pine sawdust, J. Anal. Appl. Pyrolysis 100 (2013) 26–32, https://doi.org/10.1016/j.jaap.2012.11.009.

[6] Y.Y. Gan, W. Chen, H.C. Ong, H. Sheen, J. Chang, T. Hsieh, T.C. Ling, Effects of dry and wet torrefaction pretreatment on microalgae pyrolysis analyzed by TG-FTIR and double-shot Py-GC/MS, Energy 210 (2020), 118579, https://doi.org/10.1016/j.energy.2020.118579.

[7] K.C. Chaydarreh, X. Lin, L. Guan, H. Yun, J. Gu, C. Hu, Utilization of tea oil camellia (Camellia oleifera Abel.) shells as alternative raw materials for manufacturing particleboard, Ind. Crop. Prod. 161 (2021), 113221, https://doi.org/10.1016/j.indcrop.2020.113221.

[8] L. Fu, A. Liu, China statistical yearbook- 2021, in: Output of Major Forestry Products, National Bureau of Statistics of China, Beijing, 2021, pp. 403.

[9] X. Jin, Bioactivities of water-soluble polysaccharides from fruit shell of Camellia oleifera Abel: Antitumor and antioxidant activities, Carbohydr. Polym. 87 (2012) 2198–2201, https://doi.org/10.1016/j.carbpol.2011.10.047.

[10] M. Tan, L. Luo, Z. Wu, Z. Huang, J. Zhang, J. Huang, Y. Yang, X. Zhang, H. Li, Pelletization of Camellia oleifera Abel. shell after storage: energy consumption and pellet properties, Fuel Process. Technol. 201 (2020), 106337, https://doi.org/10.1016/j.fuproc.2020.106337.

[11] Y. Xie, S. Ge, S. Jiang, Z. Liu, L. Chen, L. Wang, J. Chen, L. Qin, W. Peng, Study on biomolecules in extractives of Camellia oleifera fruit shell by GC–MS, Saudi J. Biol. Sci. 25 (2018) 234–236, https://doi.org/10.1016/j.sjbs.2017.08.006.

[12] C. Yan, Y. Liu, L. Cao, M. Xia, Q. Zhang, C. Li, R. Ruan, Oligosaccharide preparation from microwave-ethanol pretreated Camellia oleifera seed shell by enzymolysis of Agrocybe aegerita, Ind. Crop. Prod. 161 (2021), 113155 https://10.1016/j.indcrop.2020.113155.

[13] G. Lin, J. Zhu, X. Wang, Y. Chen, C. Chen, Study on extracting total polyphenol of camellia fruit shells by reflux technology, Appl. Chem. Ind. 43 (2014) 971–974, https://doi.org/10.16581/j.cnki.issn1671-3206.2014.06.042.

[14] J. Zhang, L. Hu, Z. Wang, M. Du, X. Yao, Present situation and prospective of camellia nut shells utilization, Open J. For. 5 (2015) 740–748, https://doi.org/10.4236/ojf.2015.57066.

[15] Z. Lei, S. Wang, H. Fu, W. Gao, B. Wang, J. Zeng, J. Xu, Thermal pyrolysis characteristics and kinetics of hemicellulose isolated from Camellia Oleifera Shell, Bioresour. Technol. 282 (2019) 228–235, https://doi.org/10.1016/j.biortech.2019.02.131.

[16] Y. Xie, S. Chen, X. Chi, Y. Liang, Extraction of Insoluble Dietary Fiber from Hull of Camellia oleifera Abel and Its Physicochemical Properties, J. Zhejiang Uni 39 (2013) 149–154, https://doi.org/10.3785/j.issn.1008-9209.2012.11.065.

[17] J. Zhu, Y. Zhu, F. Jiang, Y. Xu, J. Ouyang, S. Yu, An integrated process to produce ethanol, vanillin, and xylooligosaccharides from Camellia oleifera shell, Carbohydr. Res. 382 (2013) 52–57, https://doi.org/10.1016/j.carres.2013.10.007.

[18] W. Liu, M. Wang, S. Xu, C. Gao, J. Liu, Inhibitory effects of shell of Camellia oleifera Abel extract on mushroom tyrosinase and human skin melanin, J. Cosmet. Dermatol. -US 18 (2019) 1955–1960, https://doi.org/10.1111/jocd.12921.

[19] Z. Chen, J. Liu, H. Chen, Z. Ding, X. Tang, F. Evrendilek, Oxy-fuel and air atmosphere combustions of Chinese medicine residues: Performances, mechanisms, flue gas emission, and ash properties, Renew. Energy 182 (2022) 102–118, https://doi.org/10.1016/j.renene.2021.10.010.

[20] T. Deng, Z. Yu, X. Zhang, Y. Zhang, L. Chen, X. Ma, Catalytic co-pyrolysis behaviors and kinetics of camellia shell and take-out solid waste using pyrolyzer – gas chromatography/mass spectrometry and thermogravimetric analyzer, Bioresour. Technol. 297 (2020), 122419, https://doi.org/10.1016/j.biortech.2019.122419.

[21] C. Zhang, S. Li, S. Ouyang, C. Tsang, D. Xiong, K. Yang, Y. Zhou, Y. Xiao, Co-pyrolysis characteristics of camellia oleifera shell and coal in a TGA and a fixed-bed reactor, J. Anal. Appl. Pyrolsis 155 (2021), 105035, https://doi.org/10.1016/j.jaap.2021.105035.

[22] F. Fan, Y. Zheng, Y. Huang, Y. Lu, Z. Wang, B. Chen, Z. Zheng, Preparation and characterization of biochars from waste camellia oleifera shells by different thermochemical processes, Energy Fuel 31 (8) (2017) 8146–8151, https://doi.org/10.1021/acs.energyfuels.7b00269.

[23] Z. Zhang, Q. Cheng, J. Huang, X. Zhang, M. Tan, Z. Huang, N. Amaglo, Y. Suo, H. Li, Production of biochar from the combination of foaming drying and pyrolysis of sludge with the additive of Camellia oleifera shell biochar, J. Anal. Appl. Pyrolsis 160 (2021), 105350, https://doi.org/10.1016/j.jaap.2021.105350.

[24] Y. Hu, L. Qi, S. Feng, A. Bassi, C.C. Xu, Comparative studies on liquefaction of low-lipid microalgae into bio-crude oil using varying reaction media, Fuel 238 (2019) 240–247, https://doi.org/10.1016/j.fuel.2018.10.124.

[25] W. Gao, K. Chen, Z. Xiang, F. Yang, J. Zeng, J. Li, R. Yang, G. Rao, H. Tao, Kinetic study on pyrolysis of tobacco residues from the cigarette industry, Ind. Crop. Prod. 44 (2013) 152–157, https://doi.org/10.1016/j.indcrop.2012.10.032.

[26] A.W. Coats, J.P. Redfern, Kinetic parameters from thermogravimetric data, Nature 201 (1964) (1964) 68–69, https://doi.org/10.1038/201068a0.

[27] Y.S. Kim, Y.S. Kim, S.H. Kim, Investigation of thermodynamic parameters in the thermal decomposition of plastic waste−waste lube oil compounds, Environ. Sci. Technol. 44 (2010) 5313–5317, https://doi.org/10.1021/es101163e.

[28] S. Gupta, P. Patel, P. Mondal, Biofuels production from pine needles via pyrolysis: process parameters modeling and optimization through combined RSM and ANN based approach, Fuel 310 (2022), 122230, https://doi.org/10.1016/j.fuel.2021.122230.

[29] J. Fu, J. Liu, W. Xu, Z. Chen, F. Evrendilek, S. Sun, Torrefaction, temperature, and heating rate dependencies of pyrolysis of coffee grounds: Its performances, bio-oils, and emissions, Bioresour. Technol. 345 (2022), 126346, https://doi.org/10.1016/j.biortech.2021.126346.

[30] I. Mian, X. Li, Y. Jian, O.D. Dacres, M. Zhong, J. Liu, F. Ma, N. Rahman, Kinetic study of biomass pellet pyrolysis by using distributed activation energy model and coats Redfern methods and their comparison, Bioresour. Technol. 294 (2019), 122099, https://doi.org/10.1016/j.biortech.2019.122099.

[31] J. Zhang, Z. Wang, M. Du, X. Yao, L. Hu, Physicochemical properties of camellia nut shell and its thermal degradation characteristics, BioResources 10 (2015) 647–659, https://doi.org/10.15376/biores.10.1.647-659.

[32] G. Özsin, A.E. Pütün, Kinetics and evolved gas analysis for pyrolysis of food processing wastes using TGA/MS/FT-IR, Waste Manag. 64 (2017) 315–326, https://doi.org/10.1016/j.wasman.2017.03.020.

[33] Z. Ding, H. Chen, J. Liu, H. Cai, F. Evrendilek, M. Buyukada, Pyrolysis dynamics of two medical plastic wastes: Drivers, behaviors, evolved gases, reaction mechanisms, and pathways, J. Hazard. Mater. 402 (2021), 123472, https://doi.org/10.1016/j.jhazmat.2020.123472.

[34] M.A. Mehmood, G. Ye, H. Luo, C. Liu, S. Malik, I. Afzal, J. Xu, M.S. Ahmad, Pyrolysis and kinetic analyses of Camel grass (Cymbopogon schoenanthus) for bioenergy, Bioresour. Technol. 228 (2017) 18–24, https://doi.org/10.1016/j.biortech.2016.12.096.

[35] F. Zaman, N. Akhtar, Y. Guan, Y. Huang, Thermal degradation kinetic analysis and conversion of Aesculus indica to porous carbon, Ind. Crop. Prod. 153 (2020), 112555, https://doi.org/10.1016/j.indcrop.2020.112555.

[36] S.C. Turmanova, S.D. Genieva, A.S. Dimitrova, L.T. Vlaev, Non-isothermal degradation kinetics of filled with rise husk ash polypropene composites, Express Polym. Lett. 2 (2008) 133–146, https://doi.org/10.3144/expresspolymlett.2008.18.

[37] W. Chen, C. Wang, G. Kumar, P. Rousset, T. Hsieh, Effect of torrefaction pretreatment on the pyrolysis of rubber wood sawdust analyzed by Py-GC/MS, Bioresour. Technol. 259 (2018) 469–473, https://doi.org/10.1016/j.biortech.2018.03.033.

[38] L. Tian, B. Shen, H. Xu, F. Li, Y. Wang, S. Singh, Thermal behavior of waste tea pyrolysis by TG-FTIR analysis, Energy 103 (2016) 533–542, https://doi.org/10.1016/j.energy.2016.03.022.

[39] Y. Ding, O.A. Ezekoye, S. Lu, C. Wang, Thermal degradation of beech wood with thermogravimetry/Fourier transform infrared analysis, Energy Convers. Manag. 120 (2016) 370–377, https://doi.org/10.1016/j.enconman.2016.05.007.

[40] Z. Zhang, C. Wang, G. Huang, H. Liu, S. Yang, A. Zhang, Thermal degradation behaviors and reaction mechanism of carbon fibre-epoxy composite from hydrogen tank by TG-FTIR, J. Hazard. Mater. 357 (2018) 73–80, https://doi.org/10.1016/j.jhazmat.2018.05.057.

[41] E. Granada, P. Eguía, J.A. Vilan, J.A. Comesaña, R. Comesaña, FTIR quantitative analysis technique for gases. Application in a biomass thermochemical process, Renew. Energy 41 (2012) 416–421, https://doi.org/10.1016/j.renene.2011.11.020.

[42] H. Huang, J. Liu, H. Liu, F. Evrendilek, M. Buyukada, Pyrolysis of water hyacinth biomass parts: Bioenergy, gas emissions, and by-products using TG-FTIR and Py-GC/MS analyses, Energy Convers. Manag. 207 (2020), 112552, https://doi.org/10.1016/j.enconman.2020.112552.

[43] S. Zhang, Q. Dong, L. Zhang, Y. Xiong, Effects of water washing and torrefaction on the pyrolysis behavior and kinetics of rice husk through TGA and Py-GC/MS, Bioresour. Technol. 199 (2016) 352–361, https://doi.org/10.1016/j.biortech.2015.08.110.

[44] S.R. Naqvi, R. Tariq, Z. Hameed, I. Ali, M. Naqvi, W. Chen, S. Ceylan, H. Rashid, J. Ahmad, S.A. Taqvi, M. Shahbaz, Pyrolysis of high ash sewage sludge: kinetics and thermodynamic analysis using Coats-Redfern method, Renew. Energy 131 (2019) 854–860, https://doi.org/10.1016/j.renene.2018.07.094.

[45] F. Song, X. Wang, T. Li, J. Zhang, Y. Bai, B. Xing, J.P. Giesy, F. Wu, Spectroscopic analyses combined with Gaussian and Coats-Redfern models to investigate the characteristics and pyrolysis kinetics of sugarcane residue-derived biochars, J. Clean. Prod. 237 (2019), 117855, https://doi.org/10.1016/j.jclepro.2019.117855.

[46] B.B. Uzun, E. Yaman, Pyrolysis kinetics of walnut shell and waste polyolefins using thermogravimetric analysis, J. Energy Inst. 90 (2017) 825–837, https://doi.org/10.1016/j.joei.2016.09.001.

[47] A. Malika, N. Jacques, E.F. Jaafar, B. Fatima, A. Mohammed, Pyrolysis investigation of food wastes by TG-MS-DSC technique, Biomass Convers. Biorefin. 6 (2016) 161–172, https://doi.org/10.1007/s13399-015-0171-9.

[48] Y. Tonbul, Pyrolysis of pistachio shell as a biomass, J. Therm. Anal. Calorim. 91 (2007) 641–647, https://doi.org/10.1007/s10973-007-8428-6.